

## FISH: A thermal neutron imaging station at HOR Delft

Zhou, Zhou; Plomp, Jeroen; van Eijck, Lambert; Vontobel, Peter; Harti, Ralph P.; Lehmann, Eberhard; Pappas, Catherine

**DOI**

[10.1016/j.jasrep.2018.05.015](https://doi.org/10.1016/j.jasrep.2018.05.015)

**Publication date**

2018

**Document Version**

Final published version

**Published in**

Journal of Archaeological Science

**Citation (APA)**

Zhou, Z., Plomp, J., van Eijck, L., Vontobel, P., Harti, R. P., Lehmann, E., & Pappas, C. (2018). FISH: A thermal neutron imaging station at HOR Delft. *Journal of Archaeological Science*, *20*, 369-373. <https://doi.org/10.1016/j.jasrep.2018.05.015>

**Important note**

To cite this publication, please use the final published version (if applicable). Please check the document version above.

**Copyright**

Other than for strictly personal use, it is not permitted to download, forward or distribute the text or part of it, without the consent of the author(s) and/or copyright holder(s), unless the work is under an open content license such as Creative Commons.

**Takedown policy**

Please contact us and provide details if you believe this document breaches copyrights. We will remove access to the work immediately and investigate your claim.



## FISH: A thermal neutron imaging station at HOR Delft

Zhou Zhou<sup>a,\*</sup>, Jeroen Plomp<sup>a</sup>, Lambert van Eijck<sup>a</sup>, Peter Vontobel<sup>b</sup>, Ralph P. Harti<sup>b</sup>, Eberhard Lehmann<sup>b</sup>, Catherine Pappas<sup>a</sup>

<sup>a</sup> Department NPM2/RST, Faculty of Applied Sciences, Delft University of Technology, Mekelweg 15, 2629 JB Delft, The Netherlands

<sup>b</sup> Neutron Imaging and Activation Group, Laboratory for Neutron Scattering and Imaging, Paul Scherrer Institut, CH5232 Villigen PSI, Switzerland

### ABSTRACT

We report on the development of a thermal neutron imaging station FISH at the nuclear research reactor HOR, Delft University of Technology. FISH will serve as a unique new imaging facility within The Netherlands and also within at least 400 km radius, for national and international users from science and industry. This paper gives an overview on the characteristics and performance of the beamline and instrument, as determined in a collaboration with the Paul Scherrer Institut in Switzerland.

### 1. Introduction

The Hoger Onderwijs Reactor (HOR) is a 2 MW swimming-pool type reactor at Delft University of Technology, The Netherlands. It has been operated for over 50 years as a source of neutrons and positrons for education and research purposes. It is equipped with six horizontal radial beam tubes that are mainly used for neutron scattering and positron annihilation spectroscopy. The instruments around the reactor include the neutron reflectometer ROG (van Well et al., 1994), the spin-echo small angle neutron scattering facility SESANS (Rekvelde et al., 2005), the new neutron powder diffractometer PEARL (Van Eijck et al., 2016), the neutron depth profiling setup NDP as well as the 2D-ACAR positron annihilation setup. Moreover, a positron life-time setup and a small angle neutron scattering SANS instrument are being installed. The later waits for the cold neutron source, which will be installed in 2019.

In this work, we report on the development of a thermal neutron imaging station FISH at HOR. FISH has been conceived to serve a very wide range of applications in science and industrial R&D, thus responding to the needs of Dutch academia and innovative industry. In particular, Delft University of Technology houses several engineering faculties that will benefit from the neutron imaging and tomography capabilities of FISH for non-destructive investigations. Since research reactors are scarce and neutron imaging is highly demanded at such facilities, we anticipate that FISH will also attract a considerable amount of international users.

### 2. Beamline

FISH is installed at the reactor hall of HOR, and a top-view layout of

the facility is shown in Fig. 1. The neutrons are provided by the beam port L2, which has a direct view to the reactor core but is equipped with a curved stacked neutron guide system, which filters out fast neutrons (van Well et al., 1991). As seen in Fig. 1, the stacked neutron guide system provides two neutron beams: one for the neutron reflectometer ROG and the other one for the neutron imaging station FISH. The neutron guide, with a height of 60 mm and a width of 27 mm, consists of stacked glass plates coated with <sup>58</sup>Ni yielding 13 vertical micro-channels. Therefore, the beam divergence in the horizontal direction is limited by the guide to 2.03 mrad/Å. The beam size in the vertical direction is limited by placing a cylinder tube made of boron rubber with an inner diameter of 30 mm against to the exit of the guide system. A beam shutter is installed after the tube, followed by a vacuum flight tube, which reduces neutron losses due to air scattering and reduces the thermal neutron background. The sample/detector position is around 5.5 m away from the end of the stacked neutron guide, and a 2.5 cm thick boron plastic plate is placed behind the detector as a beam stop. The average neutron flux density measured at the sample position amounts to about  $3 \times 10^6 \text{ cm}^{-2} \text{ s}^{-1}$ .

As shown in Fig. 2, the open beam image has an irregular shape with straight edges in the horizontal direction due to the upstream stacked neutron guide, and rounded edges in the vertical direction due to the aperture tube. The beam intensity distribution is not homogenous either. The vertical stripes shown in the open beam are due to the stacked neutron guide which consists of vertical micro-channels. The maximum usable beam size, i.e. the field of view (FOV), at the sample position has approximately a height of 100 mm high and a width of 50 mm. It is worthwhile to mention that for objects having dimensions greater than the available FOV, radiography/tomography measurements can be

\* Corresponding author at: Mekelweg 15, 2629 JB Delft, The Netherlands.  
E-mail address: [Z.Zhou-1@tudelft.nl](mailto:Z.Zhou-1@tudelft.nl) (Z. Zhou).

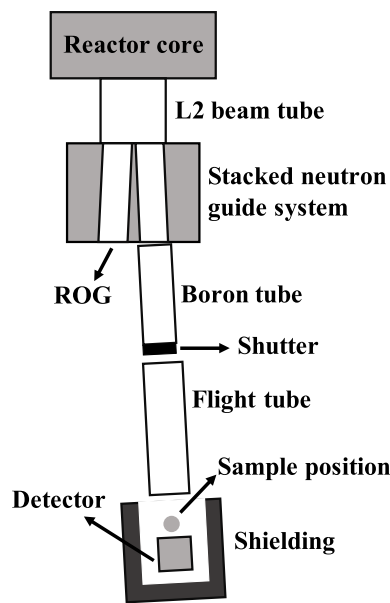


Fig. 1. Top-view layout of FISH.

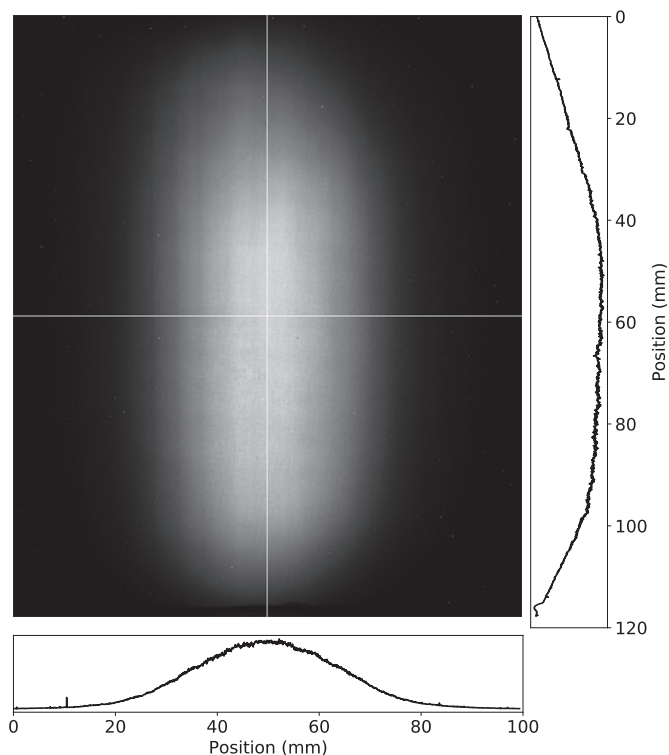


Fig. 2. An open beam image showing the beam shape, size and intensity distribution. The right and bottom are profile plots corresponding to the gray level of the vertical and horizontal lines, respectively, shown in the open beam image.

performed by taking and stitching multiple images (per angle step) to cover the whole sample.

### 3. Detector system

The detector system used for FISH is based on neutron scintillators coupled to a CCD/sCMOS camera in a light tight box. In such a system, the scintillator absorbs neutrons and emits visible light that is reflected by a mirror, travels through an optical lens and is eventually recorded

by the CCD/sCMOS sensor.

The thickness of the scintillator determines the neutron-to-light conversion efficiency but a too efficient and thick scintillator also blurs the image due to the resulting spread of light. On the other hand, the optical lens and the camera sensor determine the light capture efficiency of the detector and the nominal pixel size of the resulting images.

The scintillators are made of  ${}^6\text{LiF}/\text{ZnS}$  from RC Tritec Ltd. with thicknesses of 100  $\mu\text{m}$  and 200  $\mu\text{m}$ . Currently, a detector system provided by the company NeutronOptics Grenoble is available, which consists of a CCD camera with  $1391 \times 1039$  pixels coupled with a 50 mm lens.

For characterizing the FISH beamline, a MIDI detector system, has been borrowed from PSI and used at Delft. This system includes an Andor Neo sCMOS 16-bit camera with  $2560 \times 2160$  pixels and multiple scintillators with various thicknesses.

## 4. Performance of FISH

### 4.1. Spatial resolution

The spatial resolution of FISH setup has been evaluated by performing neutron radiography on the PSI Siemens Star test pattern. In this way, the resolution can be easily estimated by visual inspection of the visible smallest gap between the spokes (Grünzweig et al., 2007). Fig. 3 displays the normalized images obtained with different scintillator thicknesses. These images show that the achieved spatial resolution is mainly limited by the thickness of the scintillator. We note that, for a 50  $\mu\text{m}$  thick scintillator, a 100 mm macro lens must be used in order to reach a nominal optical pixel size of  $\sim 25.5 \mu\text{m}$ , while with a 50 mm lens the nominal optical pixel size is  $\sim 46 \mu\text{m}$ .

Since the thickness of the scintillator also determines the neutron detection efficiency, longer exposure times per image are required for higher spatial resolutions (thus thinner scintillators) and a compromise between the resolution and exposure time must be found. The combination of a 100  $\mu\text{m}$  thick scintillator and a 50 mm F/1.2 lens gives a spatial resolution of about 100  $\mu\text{m}$  (see Fig. 3(b)), which has an acceptable exposure time of 30–60 s and meets the needs of most applications. On the other hand, a 50  $\mu\text{m}$  thick scintillator combined with a 100 mm F/2.0 macro lens provides the best spatial resolution but at the price of less light collection efficiency. Indeed, in the latter case an exposure time of 240 s is required in order to reach a gray level of approximately 11,000 in the open beam area, resulting to a 16-bit image with a dynamic range from 0 to 65,530.

### 4.2. $L/D$ estimation

An essential parameter of neutron imaging instruments is the  $L/D$  ratio, with  $D$  the diameter of the beam aperture and  $L$  is aperture-to-sample distance (Kobayashi and Plaut, 2001). This ratio determines the image blurring, which is inherent to the beamline. This blurring results from the divergence of the neutron beam as it is transmitted through the finite-size object under investigation, and is given by:

$$d = \frac{l}{L/D},$$

where  $d$  is the blur at a sample-to-detector distance  $l$ . This blurring is thus effectively absent for thin flat objects like the Siemens star placed against the detector scintillator ( $l = 0$ ).

As we describe in Section 2, the neutron beam of FISH is provided by a guide system. An  $L/D$  ratio thus can be calculated from the geometry of the beamline:  $L/D = 5500/30 = 183$ . However, due to the upstream stacked guide system, the beamline is not a conventional pin-hole source. Therefore, it is practical to evaluate the  $L/D$  ratio from the blurring effect due to the sample-to-detector distance. For this purpose, a sharp edge object, which is a thin layer ( $\sim 150 \mu\text{m}$ ) of Gd coated on a

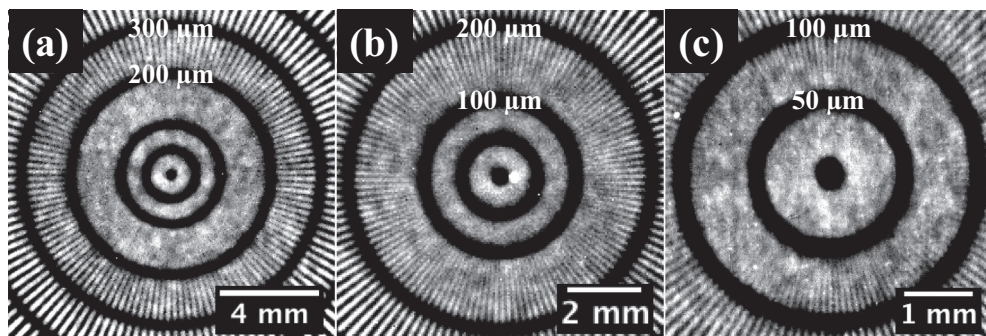


Fig. 3. Neutron radiography of the PSI Siemens Star test pattern. The images were taken using the MIDI detector system and different combinations of scintillator and lens: (a) a 200 μm thick scintillator and a 50 mm lens with exposure time 40 s, (b) a 100 μm thick scintillator and a 50 mm lens with exposure time 60 s, (c) a 50 μm thick scintillator and a 100 mm macro lens with exposure time 240 s. The images were normalized by the dark current and open beam images.

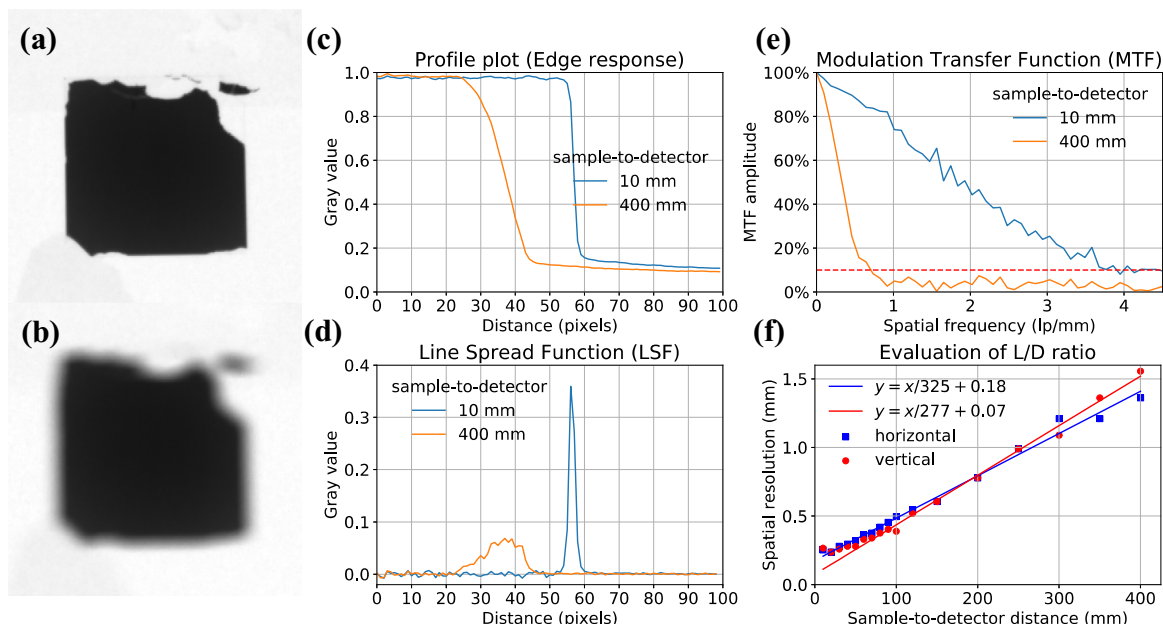


Fig. 4. Neutron radiography of a sharp edge placed at (a) 10 mm and (b) 400 mm away from the detector. The images were normalized by the dark current and open beam images. (c) The grayscale value profiles (edge response) along the vertical edge; (d) The LSF derived from the edge response; (e) The MTF obtained from the Fourier transform of LSF, and the red dash line indicates 10% MTF amplitude. (f) The spatial resolution determined from both horizontal and vertical directions plotted against the sample-to-detector distance. The data points were fitted by a straight line resulting in an evaluated L/D ratio of 325 in the horizontal direction and 277 in the vertical direction. (For interpretation of the references to colour in this figure legend, the reader is referred to the web version of this article.)

Table 1  
Measured attenuation coefficients in  $\text{cm}^{-1}$  from the contrast sample from FISH.

	Al	Cu	Pb	Ti	Fe	Ni
Theoretical <sup>a</sup>	0.11	1.0	0.37	0.59	1.2	2.1
Measured <sup>b</sup>	0.103	0.869	0.281	0.554	1.030	1.697
StdDev <sup>b</sup>	0.034	0.041	0.043	0.039	0.046	0.052
SNR <sup>b</sup>	3.03	21.2	6.53	14.2	22.4	32.6

<sup>a</sup> The values are the theoretical linear attenuation coefficients ( $\text{cm}^{-1}$ ) for thermal neutrons.

<sup>b</sup> The evaluation was performed on the reconstructed slice, and a circular Region of Interest (ROI) was defined for each inset material. The measured attenuation coefficients were determined as the mean grayscale values of the ROIs, where the standard deviations (StdDev) were obtained as well. The Signal-to-Noise Ratio (SNR) was then determined as the ratio of the mean to the standard deviation, which is a measure of the quality of the data.

Si substrate, was measured at different distances from the detector. Fig. 4 (a) and (b) show the normalized images of the sharp edge object measured at 10 and 400 mm away from the scintillator screen of the detector, respectively, indicating the blurring effect caused by the large sample-to-detector distance. Consequently, we determined the spatial resolution of the obtained images using the Modulation Transform

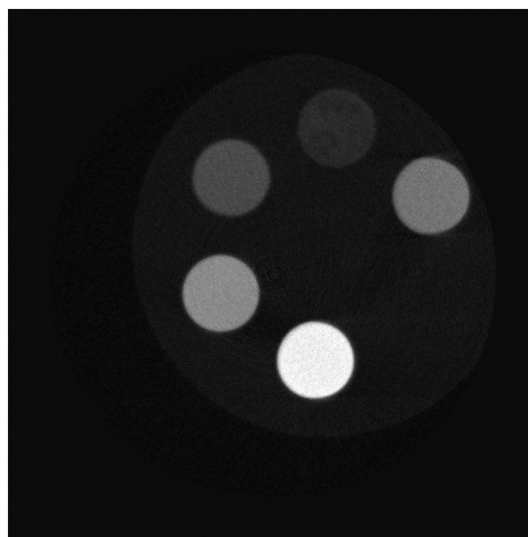


Fig. 5. A central slice of the reconstructed contrast sample.

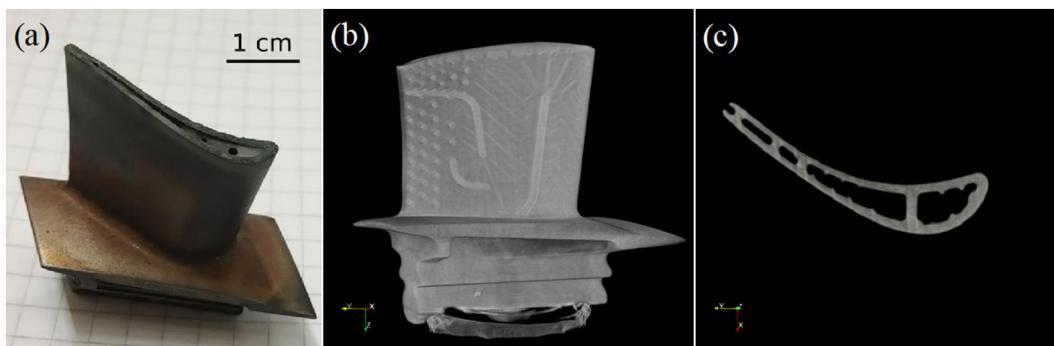


Fig. 6. (a) Photo of a turbine blade measured by neutron tomography at FISH; (b) a volume rendering and (c) a reconstructed slice from the reconstructed data.

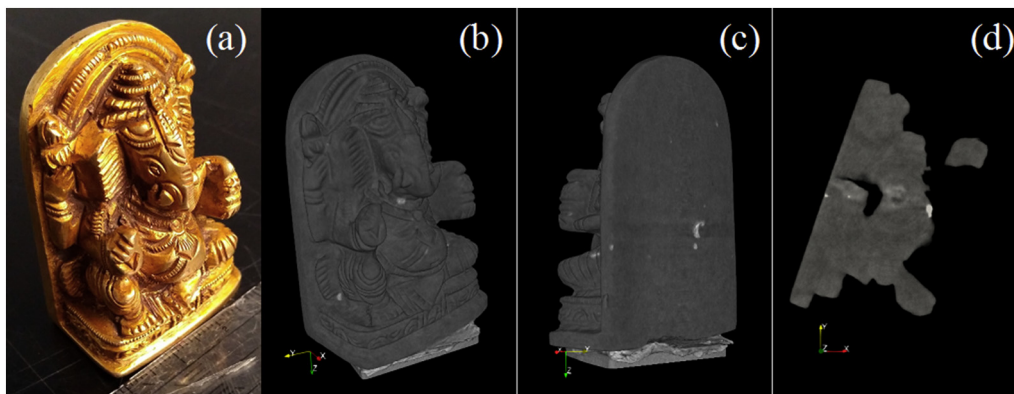


Fig. 7. (a) Photo of a brass statue measured by neutron tomography at FISH; (b) and (c) a volume rendering and (d) a reconstructed slice from the reconstructed data, showing the hollow interior of statue and some regions of high neutron attenuation.

Function (MTF) method. The steps are shown in Fig. 4(c–e): (1) the Line Spread Function (LSF) was obtained by taking the derivative of the edge response which is the profile plot of the grayscale value along the edge; (2) the MTF was derived by taking the Fourier transform of the LSF; (3) the spatial resolution was measured at 10% MTF amplitude. We note that the resolution in the horizontal and vertical directions was measured separately, since the beam collimation is not isotropic in our beamline due to the stacked neutron guide. Fig. 4 (f) shows the experimentally determined spatial resolution plotted as a function of the sample-detector distance. The corresponding value of  $L/D$  is estimated by fitting the data points to a straight line, and from the reciprocal of the linear regression slope (Baechler et al., 2002). The results lead to a  $L/D$  ratio of about 325 in the horizontal direction and 277 in the vertical direction. This result indicates that, at the current sample position, FISH is a very competitive imaging setup (Lehmann and Ridikas, 2015).

#### 4.3. Tomography performance

The neutron tomography performance of FISH has been evaluated by measuring a reference sample from PSI. The sample was a cylinder of aluminum with 6 insets of different materials, listed in Table 1. The detailed description of the sample can be found in (Kaestner et al., 2013). The tomography measurement was performed with the MIDI detector system and a 100  $\mu\text{m}$  thick scintillator and a 50 mm lens was used for leading to a nominal optical pixel size of 46  $\mu\text{m}$ . The tomographic measurements consisted of 401 projections, 10 dark current and 10 open beam images, and each image had an exposure time of 60 s. The tomographic reconstruction was performed using Octopus Reconstruction 8. (Dierick et al., 2004). Fig. 5 shows a central slice of the reconstructed data. The attenuation coefficients of the insets were evaluated using the approach described in (Kaestner et al., 2013). The results are listed in Table 1 and show that the 6 different materials can

be well discriminated from the tomography measurement. Furthermore, the measured attenuation coefficients are very comparable to the expected values. Indeed, all the measured values are lower than the theoretic ones, which is due to the effect of scattering and beam hardening.

The high quality of the tomography experiments performed on FISH is illustrated by Figs. 6 and 7. These show reconstructed data from a turbine blade and a brass statue, respectively. The reconstructed images are of high quality and can be used to investigate the structural details of the samples.

## 5. Summary and outlook

The thermal neutron imaging station FISH at Delft is in operation since 2017 and allows neutron radiography and tomography measurements for internal and external users. The performance of the setup has been tested by radiography and tomography measurements on reference objects. FISH has a maximum useable beam size of 100 mm  $\times$  50 mm, and an estimated  $L/D$  ratio of 325, and 277 in the horizontal and the vertical directions, respectively.

The team around FISH is establishing a connection between the neutron imaging technique and the Dutch Museums and Cultural Heritage field. One can foresee the growing interest and use of neutron imaging for non-destructive investigation of cultural heritage objects in the Netherlands. We also collaborate with internal and external partners to extend the range of experiments and applications of FISH. These include materials science and engineering, archaeology, civil engineering and plant physiology. Additional collaborations include Photonis Technologies S.A.S. (Pinto et al., 2017) and Amsterdam Scientific Instruments on the development of the detector system. In the future, other imaging capabilities will be explored on the FISH beamline, such as dark-field imaging with gratings.

## Acknowledgement

We thank Sara Creange from the Rijksmuseum for providing the brass statue for the neutron tomography measurement. We thank C.F. de Vroege and F.T.C.J. Naastepad for their kind support on the LabView interface controlling the sample stage of FISH.

## References

- Baechler, S., Kardjilov, N., Dierick, M., Jolie, J., Kühne, G., Lehmann, E., Materna, T., 2002. New features in cold neutron radiography and tomography - Part I: Thinner scintillators and a neutron velocity selector to improve the spatial resolution. *Nucl. Instruments Methods Phys. Res. Sect. A Accel. Spectrometers, Detect. Assoc. Equip.* 491, 481–491. [http://dx.doi.org/10.1016/S0168-9002\(02\)01238-X](http://dx.doi.org/10.1016/S0168-9002(02)01238-X).
- Dierick, M., Masschaele, B., Van Hoorbeke, L., 2004. Octopus, a fast and user-friendly tomographic reconstruction package developed in LabView®. *Meas. Sci. Technol.* 15, 1366–1370. <http://dx.doi.org/10.1088/0957-0233/15/7/020>.
- Grünzweig, C., Frei, G., Lehmann, E., Kühne, G., David, C., 2007. Highly absorbing gadolinium test device to characterize the performance of neutron imaging detector systems. *Rev. Sci. Instrum.* 78. <http://dx.doi.org/10.1063/1.2736892>.
- Kaestner, A.P., Lehmann, E.H., Hovind, J., Radebe, M.J., De Beer, F.C., Sim, C.M., 2013. Verifying neutron tomography performance using test objects. In: *Physics Procedia*. 137. Elsevier B.V., pp. 128. <http://dx.doi.org/10.1016/j.phpro.2013.03.016>.
- Kobayashi, H., Plaut, R.H., 2001. Beam formation and characterization for neutron radiography. *Nondestruct. Test. Eval.* 16, 121–129. <http://dx.doi.org/10.1080/10589750108953069>.
- Lehmann, E.H., Ridikas, D., 2015. Status of neutron imaging - activities in a worldwide context. *Phys. Procedia* 10–17. <http://dx.doi.org/10.1016/j.phpro.2015.07.001>.
- Pinto, S.D., Ortega, R., Ritzau, S., Pasquale, D., Laprade, B., Mrotek, S., Gardell, S., Zhou, Z., Plomp, J., van Eijck, L., Bilheux, H., Dhiman, I., 2017. Neutron imaging and tomography with MCPS. *J. Instrum.* 12, C12006. <http://dx.doi.org/10.1088/1748-0221/12/12/C12006>.
- Rekvelde, M.T., Plomp, J., Bouwman, W.G., Kraan, W.H., Grigoriev, S., Blaauw, M., 2005. Spin-echo small angle neutron scattering in Delft. *Rev. Sci. Instrum.* 76. <http://dx.doi.org/10.1063/1.1858579>.
- Van Eijck, L., Cussen, L.D., Sykora, G.J., Schooneveld, E.M., Rhodes, N.J., Van Well, A.A., Pappas, C., 2016. Design and performance of a novel neutron powder diffractometer: PEARL at TU Delft. *J. Appl. Crystallogr.* 49, 1398–1401. <http://dx.doi.org/10.1107/S160057671601089X>.
- van Well, A.A., De Haan, V.O., Rekvelde, M.T., 1991. Stacked neutron guides at IRI Delft. *Neutron News* 2.
- van Well, A.A., de Haan, V.O., Fredrikze, H., 1994. ROG, the new neutron reflectometer at IRI, Delft. *Phys. B Phys. Condens. Matter* 198, 217–219. [http://dx.doi.org/10.1016/0921-4526\(94\)90163-5](http://dx.doi.org/10.1016/0921-4526(94)90163-5).